

# Effects of the window openings on the micro-environmental condition in a school bus



Fei Li <sup>a,\*</sup>, Eon S. Lee <sup>b</sup>, Bin Zhou <sup>a</sup>, Junjie Liu <sup>c</sup>, Yifang Zhu <sup>b</sup>

<sup>a</sup> Department of HVAC, College of Urban Construction, Nanjing Tech University, Nanjing, 210009, China

<sup>b</sup> Department of Environmental Health Sciences, Jonathan and Karin Fielding School of Public Health, University of California, Los Angeles, CA, 90095-1772, USA

<sup>c</sup> Tianjin Key Lab of Indoor Air Environmental Quality Control, School of Environmental Science and Engineering, Tianjin University, Tianjin, 300072, China

## HIGHLIGHTS

- Proposed a method to simulate the infiltration airflow through window gaps.
- Analyzed the effect of different side-window openings on the airflow pattern.
- Measured BC and UFPs concentration inside with different window openings.

## ARTICLE INFO

### Article history:

Received 17 April 2017

Received in revised form

20 August 2017

Accepted 22 August 2017

Available online 23 August 2017

### Keywords:

Micro-environment

Air pollution

Window position

Airflow pattern

CFD

## ABSTRACT

School bus is an important micro-environment for children's health because the level of in-cabin air pollution can increase due to its own exhaust in addition to on-road traffic emissions. However, it has been challenging to understand the in-cabin air quality that is associated with complex airflow patterns inside and outside a school bus. This study conducted Computational Fluid Dynamics (CFD) modeling analyses to determine the effects of window openings on the self-pollution for a school bus. Infiltration through the window gaps is modeled by applying variable numbers of active computational cells as a function of the effective area ratio of the opening. The experimental data on ventilation rates from the literature was used to validate the model. Ultrafine particles (UFPs) and black carbon (BC) concentrations were monitored in "real world" field campaigns using school buses. This modeling study examined the airflow pattern inside the school bus under four different types of side-window openings at 20, 40, and 60 mph (i.e., a total of 12 cases). We found that opening the driver's window could allow the infiltration of exhaust through window/door gaps in the back of school bus; whereas, opening windows in the middle of the school bus could mitigate this phenomenon. We also found that an increased driving speed (from 20 mph to 60 mph) could result in a higher ventilation rate (up to 3.4 times) and lower mean age of air (down to 0.29 time) inside the bus.

© 2017 Elsevier Ltd. All rights reserved.

## 1. Introduction

School buses transport 25 million children in the United States every day (U.S.EPA, 2012). Inside a school bus, children are exposed to air pollutants such as ultrafine particles (UFPs), black carbon (BC) and polycyclic aromatic hydrocarbon (PAH) at levels higher than surrounding environments (Rim et al., 2008; Sabin et al., 2004; Zhang and Zhu, 2010). Children are more vulnerable to these

pollutants because they have narrow lung airways, immature immune systems, and high metabolism rates in comparison to those in adults (Kim, 2004; Mott et al., 1997). Improving school bus cabin air quality may be good for children's health.

Air pollutants inside school buses come from self-pollution of school bus itself in addition to on-road air pollution from surrounding vehicles. Up to 0.3% of school buses' own exhaust can be self-pollution which contributes approximately 25% of the in-cabin BC concentration (Behrentz et al., 2004). Infiltration pathway includes the leaks in the back surface of school bus and consequently result in self-pollution (Li et al., 2015; Maybee et al., 2010). Infiltration of its own exhaust is known to occur through the window/

\* Corresponding author.

E-mail address: [faylee@njtech.edu.cn](mailto:faylee@njtech.edu.cn) (F. Li).

door gaps of school buses; therefore, wind direction and window condition determine the change of air pollutant concentrations inside school buses (Zhang et al., 2013). Counter-intuitively, when the windows are closed, moving school buses experienced an increased level of self-pollution (i.e., SF<sub>6</sub> as an tracer gas indicator), potentially because of the decreased ventilation rate (i.e., air exchange) and the increased infiltration of its own exhaust (Sabin et al., 2004; Zhang and Zhu, 2010). Thus, the air quality inside a school bus largely depends on both ventilation (*intended*) and own exhaust infiltration (*unintended*) that change not only airflow pathways, but also spatial distribution of air pollutants.

Numerical simulation has been used to investigate the distribution of airflow inside bus cabins. Previous numerical modeling studies (Hu et al., 2012; Kale et al., 2007) showed the ambient air penetrating through the rear windows, moving towards the front, and finally exiting through the front windows. They also found relatively higher air turbulence in the rear section than other sections of the bus. In another numerical modeling study, Zhu et al. (2010) conducted computational fluid dynamics (CFD) modeling analysis to determine the distributions of residual lifetime and the age of air inside public transit buses with all doors and windows closed. Overall, previous studies have investigated either air quality or airflow pattern for buses. However, none of the studies have considered different window positions.

Focusing on self-pollution, this study aims to evaluate the change of airflow patterns under four window conditions at three driving speeds. For the gap in this area, we examined effects of window openings and driving speeds on the airflow pattern and air quality inside the bus cabin. Numerical modeling analyses were conducted to simulate the infiltration airflow through the gap of windows and the model results were validated with experimental measurements. This numerical and experiment method provide useful tools and information to better understand air quality inside school buses.

## 2. Methodology

### 2.1. Bus geometry

Fig. 1 (a) illustrates the geometry of a school bus digitized for model analysis. The dimensions of the bus cabin are 7.6 m (L) × 2.2 m (W) × 2.4 m (H), and the cabin includes eight rows and 41 seats. The window gaps and studied window positions are also marked, and no air-conditioning (AC) is used. Fig. 1(b) shows the top view of the bus cabin. The air velocity and the age of air distributions were calculated and compared at the cross sections MM' and NN', shown in Fig. 1(b), under different modeling scenarios.

### 2.2. Numerical methods

#### 2.2.1. Numerical model and discretization schemes

The Reynolds-averaged Navier-Stokes (RANS) equations with the k-ε model were employed to solve the airflow field of the bus cabin. Previous studies (Li et al., 2016; Lin et al., 2012; Zhu et al., 2010) have found RANS k-ε model agree well with experimental data of air velocity and concentration in bus and aircraft cabins. The governing equation for the k-ε model can be written in a general form:

$$\frac{\partial(\rho\phi)}{\partial t} + \nabla \cdot (\rho \vec{u} \phi) = \nabla \cdot (\Gamma_{\phi, \text{eff}} \nabla \phi) + S_{\phi} \quad (1)$$

where,  $\phi$  is the variable representing air velocity, energy (i.e., enthalpy), turbulence kinetic energy and turbulence dissipation, and species concentration;  $\Gamma_{\phi, \text{eff}}$  is the effective diffusion

coefficient;  $S_{\phi}$  is the source term;  $t$  is the time; and  $\vec{u}$  is the Reynolds-averaged velocity vector. When  $\phi$  is equal to 1,  $\Gamma_{\phi, \text{eff}}$  and  $S_{\phi}$  are equal to zero. ANSYS theory guide (Ansys, 2011) provides the terms and coefficients associated with each individual variable ( $\phi$ ) in details.

In this study, the age of air is the averaged time of the fresh air to transport to a specified location. The age of air is an estimate of the ventilation efficiency in the room that is calculated under steady-state condition by solving the following scalar equation:

$$\nabla \cdot (\rho \vec{u} \tau - \Gamma_{\tau} \nabla \tau) = S_{\tau} \quad (2)$$

where,  $\tau$  is the age of air (AA (s));  $\rho \vec{u}$  is the mass airflow rate;  $\Gamma_{\tau} = 2.88\rho \times 10^{-5} + \frac{\mu_{\text{eff}}}{0.7}$  (Abanto et al., 2004) is the diffusion coefficient of  $\tau$ ,  $\mu_{\text{eff}}$  is the effective dynamic viscosity; and  $S_{\tau}$  is the source term that is a function of the density of air-pollutant mixture. This equation assumes that the scalar contaminant is generated uniformly and continuously throughout the computational domain and contaminate the air gradually as it leaves the opening until reaches the specific location.

A commercial software, ANSYS Fluent (version 14.0), was used as the numerical solver. For RANS k-ε model, this study applied the SIMPLE algorithm to couple pressure and velocity. "PRESTO!" discretization scheme was used for pressure and second-order upwind discretization scheme was used for all other variables. The residual criteria of iteration were below  $10^{-3}$  for continuity, momentum equations, and species concentration. In addition, the standard wall treatment was adopted for this study because the calculated  $y$  plus value almost fell within the range of 30–300; and when  $y$  plus < 11.225, ANSYS Fluent applies to the laminar stress-strain relationship.

#### 2.2.2. Grid and boundary conditions

In this study, the air infiltration through the window gaps was accounted for. It is difficult to acquire accurate measure of window gaps (typically less than 5 mm). Considering the trade-off between computational cost and the number of computational cells to describe the geometry, this study set 5 mm for the window leakage gap. This assumption, however, potentially imposes model overestimation for the ventilation rate. Zhang et al. (2009) proposed a simple method to address a similar problem. They assigned the actual velocities on a certain percentage of boundary cells with the others blocked randomly to simulate a complex diffuser. This study adopted this method to prevent overestimation. The actual relative pressures were assigned to a certain percentage of boundary cells only, while the other boundary cells were deactivated, in order to compute the velocity of infiltration air flow through a window gap. For example, Fig. 2 shows the open (i.e., active) and blocked (i.e., deactivated) cells at a window gap. Random (i) is a function to generate a random number evenly distributed between 0 and 1;  $i$  is the cell index ranging from 1 to  $N$ ; and,  $k$  is the effective area ratio of the boundary cells. Note that  $N$  is large enough to obtain the grid-independent results and make the effective area equal to  $k$ .

A very fine mesh with a size of 5 mm was used for the window gap, and the mesh size had a growth rate of two (Fig. 3). The grid quality was ensured with the orthogonal quality higher than 0.18 for all meshes. Grid convergence index (GCI) recommended later by Roache (1994) was used to calculate the relative error among different grids.

$$\text{GCI} = F_s \frac{\epsilon_{\text{rms}}}{r^p - 1} \quad (3)$$

where  $F_s = 3$ ,  $p = 2$ , and  $r$  is the ratio of the amount of the fine grids to that of coarse grids.  $\epsilon_{\text{rms}}$  is defined as:

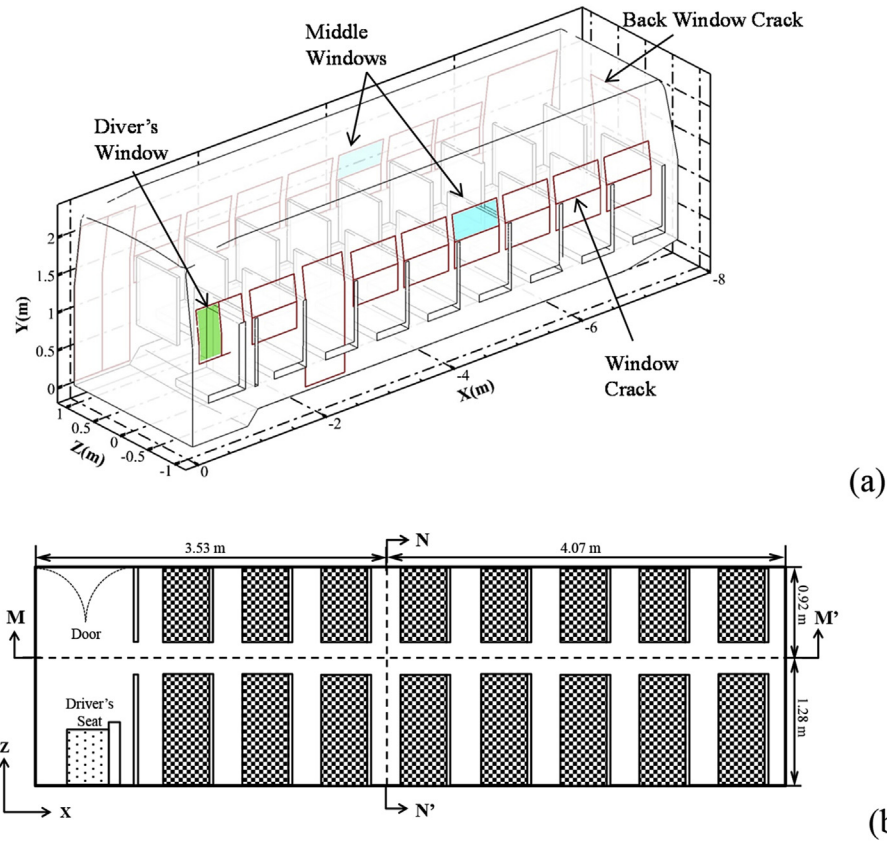


Fig. 1. Geometrical characteristic of the school bus. (a) Digital geometry model used in CFD. (b) Top view of the bus cabin.

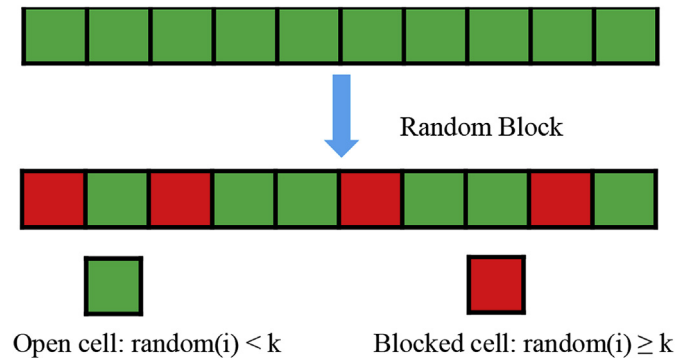


Fig. 2. Schematic of the boundary setting method for the window gap. (k: effective area ratio, i: cell index).

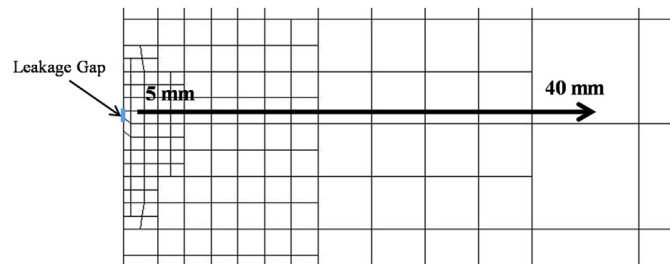


Fig. 3. Mesh size at the window leakage gap.

$$\epsilon_{rms} = \left( \frac{\sum_{i=1}^n \epsilon_{i,Q}^2}{n} \right)^{\frac{1}{2}} \quad (4)$$

where  $\epsilon_{i,Q}$  is defined as:

$$\epsilon_{i,Q} = \frac{Q_{i,coarse} - Q_{i,fine}}{Q_{i,fine}} \quad (5)$$

$Q$  is airflow rate variable. The solutions of  $Q$  at different window gaps and openings are selected in coarse (80 mm in domain) and fine (40 mm in domain) grid cases. The GCI value is <10%, indicating the coarse grid is fine enough. The total number of hexahedron cells was 1.7 million. Additionally, in other modeling studies on bus cabins (Zhu et al., 2010, 2012), the number of computational cells were 1.1 million in flow field.

For the studied side-window position, as seen in Fig. 1(a), the selected scenarios should be the representativeness. In real-world conditions, due to different seasons and passengers, different combinations of window openings are too many. Based on our previous study on the surface pressure distribution (Li et al., 2015), the relative pressure is lowest at the driver's window but highest at the middle windows among potential infiltration areas (Fig. S1), indicating that these two window opening positions have greatest impact on airflow patterns inside the cabin. Therefore, two key positions were selected: the driver's window and middle windows. The boundary condition of the gaps and windows was set as the pressure inlet with the input of relative pressure previously estimated for the external surface of school bus envelop (see Li et al. (2015) for more details). Three driving speeds were chosen to simulate school bus operation on residential streets (20 mph), on

arterial roads (40 mph), and on highways (60 mph). At each driving speed, four window scenarios (Case A: all windows closed; Case D: only driver's window open; Case DM: both driver's and middle windows open; and Case M: only middle windows open) were investigated to analyze their effects on the airflow patterns in the bus cabin. Table 1 summarizes each of the 12 modeling scenarios.

### 2.3. Experimental methods

In order to examine the hypothesis derived from the CFD simulation, a field experiment was conducted using two school buses without AC. The measurements were conducted inside two type-C school buses of the same kind evaluated in this modeling study. A type-C school bus is constructed utilizing a chassis with a hood and front fender assembly. The school bus was driven on local roadways ( $30 \pm 29$  km/h) and freeways ( $87 \pm 37$  km/h) during morning and afternoon commuting (7–8 h/day for each school bus). In each case, to test the effect of the side window openings on the cabin air quality, three scenarios were examined: Case A, Case D, and Case M. UFPs and BC concentration inside and outside the school buses are monitored because they are the air pollutant constituents primarily from traffic emissions (Vu et al., 2015). The UFPs concentrations were recorded with two condensation particle counters (CPCs, Model 3007, TSI Inc., St. Paul MN); and two aethalometers (Models AE-22 and AE-42, Magee Scientific Co.,

Berkeley, CA) measured BC concentrations. The details about experimental measurements are well described in our previous study (Lee et al., 2015).

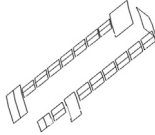
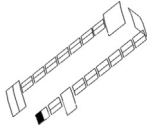
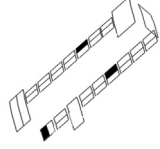
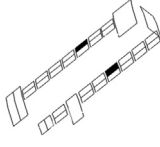
## 3. Results and discussion

### 3.1. Validation of the numerical method

In the CFD model, the key parameter for the boundary setting was the effective area ratio of the gap boundary cells ( $k$ ). Fitz et al. (2003) measured the time constant of some school buses with windows closed. Two of the school buses were evaluated in their study, and the time constant (i.e., the ratio of volume to infiltration airflow rate) was 88 s at driving speed of 40 mph. Because their buses had the similar geometry as the school bus selected in this study, we used their data for model validation and  $k$  value optimization. The surface pressure of school bus envelop was first predicted at the speed of 40 mph and assigned as the boundary condition for the gaps of windows. Then, the effective area ratio  $k$  was optimized to match with the time constant (i.e., 88 s) and determined at 0.6 for the school bus evaluated in this study.

To validate the model and  $k$  value, the time constant at the speed of 20 mph was further calculated with the effective area ratio of 0.6 to be compared with the experimental data presented in Fitz et al. (2003). The measured time constants of the two buses at the speed

**Table 1**  
Summary of modeling scenarios.

Modeling scenarios			Model predictions				
Case nO.	Schematic view	Speeds	$\bar{A}\bar{A}$ (s)	$\tau$ (s)	$Q_{\text{total}}$ (m <sup>3</sup> /s)	$Q_{\text{back-in}}$ (m <sup>3</sup> /s)	$Q_{\text{cross}}$ (m <sup>3</sup> /s)
A20 A40 A60		20 mph	130	172	0.20	0	0.10
		40 mph	139	85	0.41	0	0.12
		60 mph	40	50	0.68	0	0.32
D20 D40 D60		20 mph	71	74	0.47	0.010	0.29
		40 mph	34	36	0.96	0.018	0.58
		60 mph	22	22	1.57	0.035	1.00
DM20 DM40 DM60		20 mph	49	53	0.65	0	0.56
		40 mph	24	26	1.33	0	1.10
		60 mph	14	15	2.28	0	1.93
M20 M40 M60		20 mph	91	122	0.28	0	0.19
		40 mph	47	59	0.58	0	0.41
		60 mph	31	35	0.99	0	0.69

$\bar{A}\bar{A}$ : Average value of age of air for the whole cabin.

$\tau$ : Time constant.

$Q_{\text{total}}$ : Ventilation rate of the cabin.

$Q_{\text{back-in}}$ : Infiltration airflow rate that penetrated into the cabin through gaps on the back surface.

$Q_{\text{cross}}$ : Airflow rate through the cross section NN'.



of 20 mph were in the range from 120 s to 278 s. Different time constants were measured because the bus ventilation rate was more sensitive to the ambient environment at a lower speed. The predicted time constant through the CFD model was 172 s, and it was within the range of experimental data (120 s–278 s), suggesting the boundary setting method was reasonable.

### 3.2. Simulation results

#### 3.2.1. Effect of the side-window position

Model predictions were compared to examine the airflow characteristics under four different scenarios of open/close windows at the speed of 40 mph. Table 1 exhibits the schematic view for the detailed location and position of open/close windows under each scenario. The airflow in the cabin, the air velocity in the cross section NN' and the age of air in the longitudinal section MM' were calculated.

Fig. 4 shows the airflow streamlines inside the school bus cabin under different window conditions. For clarity, Fig. 4 only shows the streamlines from the left and back. In each scenario, the estimated airflow streamlines suggested that the ambient air mostly enters the cabin through the middle window gaps or openings and exits through the front and rear outlets. This phenomenon resulted from the distribution of relative pressure on the surface of school bus envelop. As shown in Li et al. (2015) (Fig. S1), the surface pressure becomes relatively high on the middle section of school buses, while it becomes relatively lower in the front and rear sections. Therefore, the infiltration of ambient air occurred through the window gaps or openings in the middle, and exited through the front and rear of the school bus. This phenomenon was especially noticeable for Case DM due to its large openings (Fig. 4(c)). Li et al. (2015) found that the exhaust of school bus can enter the cabin through gaps on the back surface. When the driver's window is open (Fig. 4(b)), the airflow path from the back surface shows similar findings. The driver's window is located at low surface pressure region relative to other windows; and thus, opening driver's window can promote infiltration through the other area of leaks where surface pressure is greater. Accordingly, as shown in

Table 1, the infiltration through the back surface (i.e.,  $Q_{\text{back-in}}$ ) is especially high for Case D.

Fig. 5 shows the distribution of air velocity at the cross section NN'. The contours in Fig. 5 are plotted with predicted velocity in the longitudinal (x) direction, and the vectors in Fig. 5 are plotted with model predictions of cross velocity (i.e., z and y-velocity). The longitudinal velocity (positive x direction) on the sides were lower than that in the middle due to the block of seats, and the distribution was not symmetrical because of the asymmetrical interior geometry and infiltration/ventilation. Based on the distribution of surface relative pressure, the inner-bus pressure level ranged from the highest relative pressure to the lowest relative pressure. This inner-bus pressure difference could move the air inside liking a “pump”. For Case DM, the longitudinal velocity (Fig. 5(c)) and the flow rate through the cross section NN' (Table 1) are the highest ( $1.1 \text{ m}^3/\text{s}$ ). Illustrated by the airflow in Fig. 4(c), most of the ambient air enters the cabin through the middle windows and exits through the driver's window. Opening the driver's and middle windows simultaneously can led to an observable “pumping” effect, which transports the air from back to front like a pump. In contrast, for Case A, the longitudinal velocity (Fig. 5(a)) and the flow rate through the cross section NN' (Table 1) are the lowest ( $0.12 \text{ m}^3/\text{s}$ ) because the air only enters and exits through the gaps. For Case D (Fig. 5(b)), the longitudinal velocity is lower than that for Case DM, and the flow rate through the cross section NN' (Table 1) is slightly higher than that for Case M. Further, the magnitude of cross velocity in each case was lower than its longitudinal velocity because the air jets from the window gaps attenuated rapidly in the cabin.

Fig. 6 provides the age of air distributions in the longitudinal section MM'. Corresponding to the airflow illustrated in Fig. 4, the age of air in the middle section of the cabin was lower for all scenarios because most of the air entered through the middle gaps and windows. The age of air for the scenario for Case DM (Fig. 6(c)) was the lowest due to its observable “pump” effect and high ventilation rate ( $1.33 \text{ m}^3/\text{s}$  in Table 1). The age of air was the highest for Case A (Fig. 6(a)) because of the low ventilation rate ( $0.41 \text{ m}^3/\text{s}$  in Table 1). The age of air for Case D was lower than that for Case M (Table 1) due to its higher ventilation rate ( $0.96 \text{ m}^3/\text{s}$  vs.  $0.58 \text{ m}^3/\text{s}$ ).

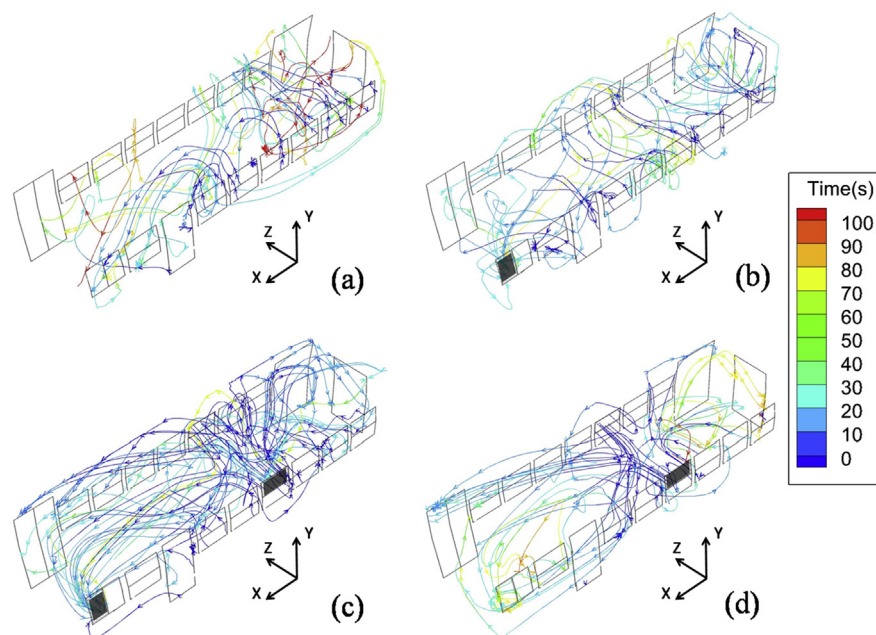
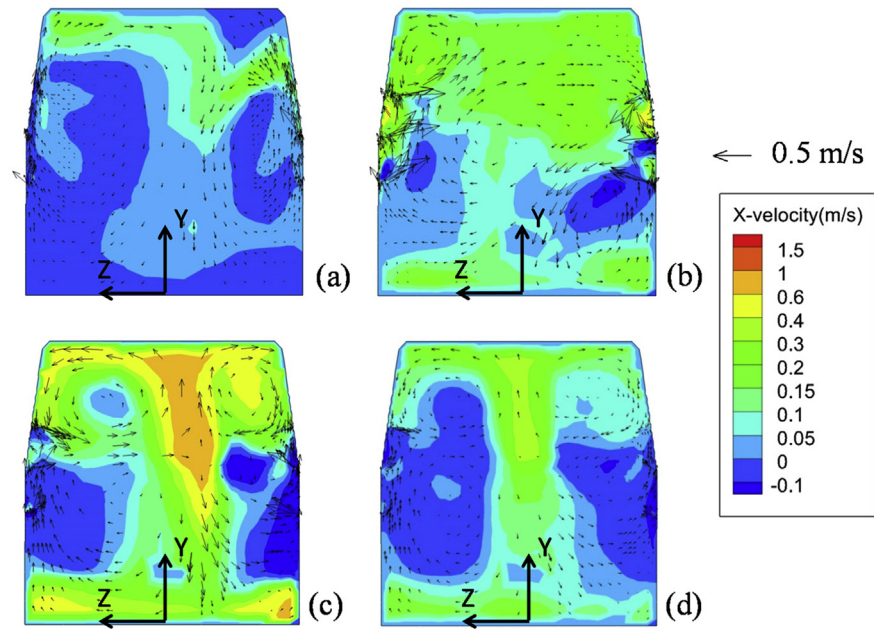
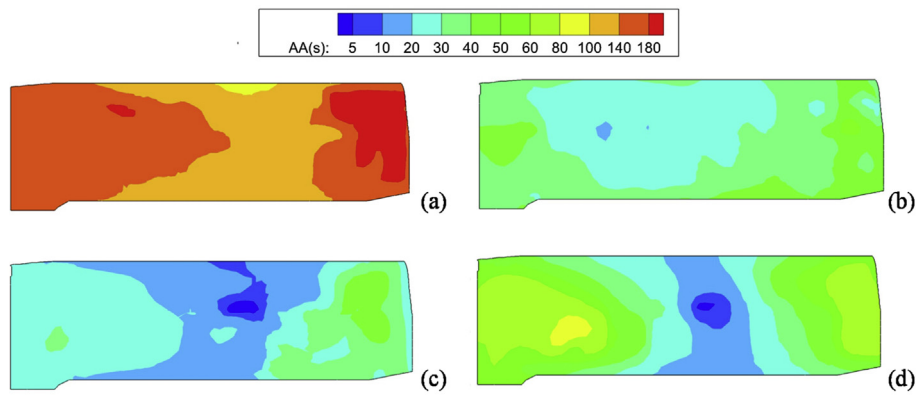


Fig. 4. Airflow patterns in the cabin for: (a) all windows closed, (b) only driver's window open, (c) both driver's and middle windows open, (d) only middle windows open.



**Fig. 5.** Predicted velocity distribution in the cross section NN' for: (a) all windows closed, (b) only driver's window open, (c) both driver's and middle windows open, (d) only middle windows open.



**Fig. 6.** Age of air (AA (s)) distribution in the longitudinal section MM' for: (a) all windows closed, (b) only driver's window open, (c) both driver's and middle windows open, (d) only middle windows open.

### 3.2.2. Effects of the bus speed

Fig. 7 provides the airflow patterns at 20, 40, and 60 mph for Case D in which only the driver's window is open. The colored contour represents the residual time of the air estimated at each speed; in the cabin, the residual time of the air decreases at

increasing speed. The higher speed increased ventilation and infiltration airflow rates through the gap of the back surfaces. See Table 1 for the numeric data.

In cross-sectional plane NN', Fig. 8 shows that the longitudinal and cross velocity around the window gaps increases at higher

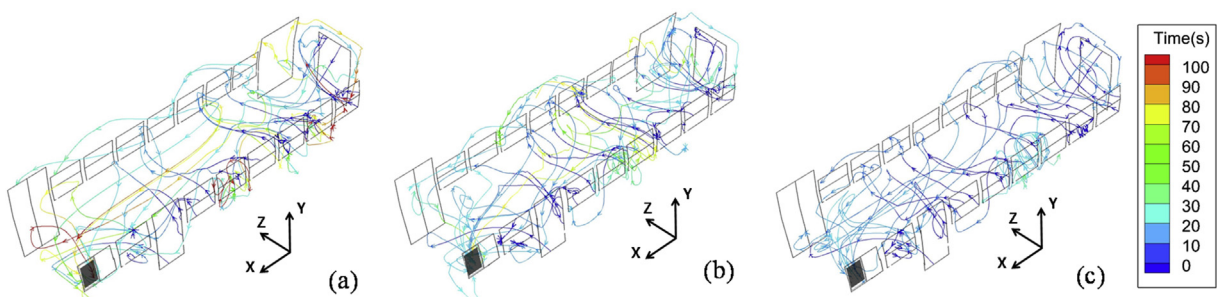


**Fig. 7.** Residual time of the air in the cabin for only the driver's window open scenario at the speed of (a) 20 mph, (b) 40 mph and (c) 60 mph.

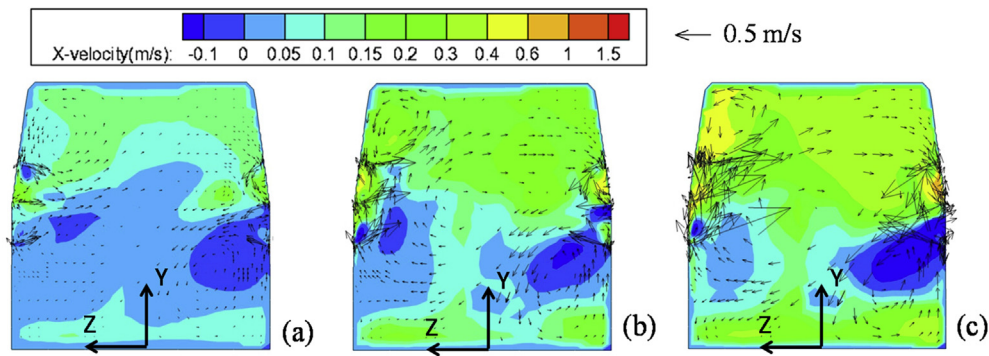


Fig. 8. Predicted velocity distribution in the cross section NN' for only driver's window open scenario at the speed of (a) 20 mph, (b) 40 mph and (c) 60 mph.

speeds. This indicates that a higher speed will likely result in a more observable “pump” effect and suck more external air. As shown in Fig. 9, the age of air in the cabin decreases as the bus speed increases, because higher ventilation rate is associated with higher speeds.

Table 1 summarizes the predicted parameters including the average value of age of air for the whole cabin ( $\bar{AA}$ ), time constant ( $\tau$ ), total ventilation rate ( $Q_{total}$ ), airflow rate which infiltrated into the cabin through gaps on the back ( $Q_{back-in}$ ) and airflow rate through the cross section ( $Q_{cross}$ ). Based on the aforementioned simulated results, it becomes clear that the window openings have a substantial effect on the airflow pattern in the bus cabin. For Case D, the air could enter through the back gaps. The ventilation rate of the cabin and the flow rate through the cross section NN' were the highest for Case DM. The tendency is similar at other speeds as

shown in Table 1. Results in Figs. 7–9 also suggested the bus speed has an effect on the airflow characteristic, which determines the leakage flow rate. A higher speed will induce a more observable “pump” effect and suck more air from the outside.

A sensitivity analysis was employed to analyze the contribution of bus speed based on changing the speed magnitude (doubled or quadrupled). For the ventilation rate, as shown in Fig. 10(a), it is increased to 2 times with changing the speed from 20 mph to 40 mph, while increased to about 3.4 times with changing the speed from 20 mph to 60 mph. It is indicated the relationship between speed and ventilation rate is not linear and the influence from speed is more significant when the speed is higher. The sensitivity of ventilation to the bus speed was almost the same for different window opening scenarios. For the age of air, as shown in Fig. 10(b), it is decreased to 0.5 time with changing the speed from 20 mph to

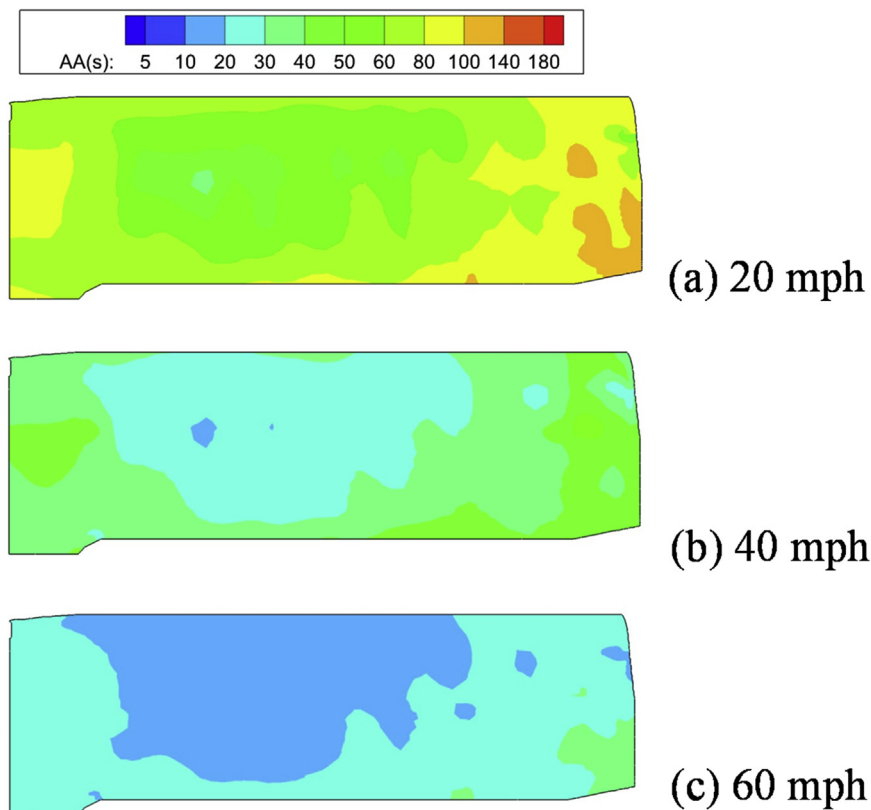


Fig. 9. Age of air (AA (s)) distribution in the longitudinal section MM' for only driver's window open case at the speed of (a) 20 mph, (b) 40 mph and (c) 60 mph.

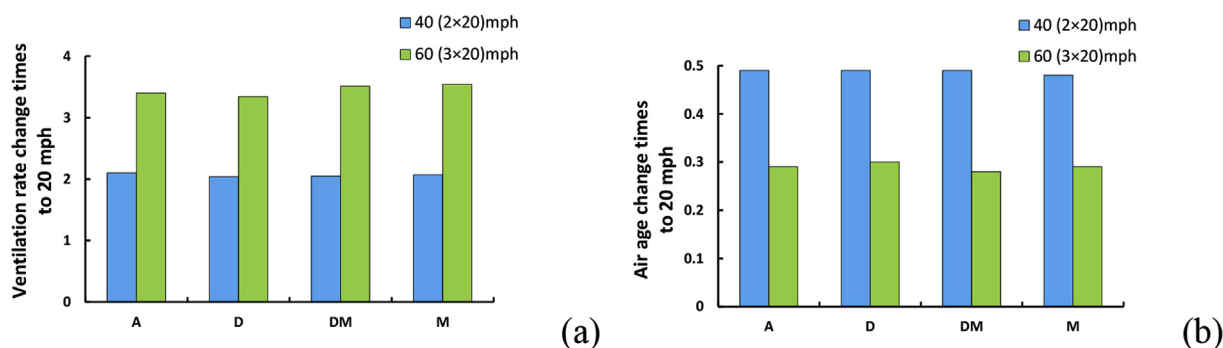


Fig. 10. Sensitivity of ventilation rate (a) and age of air (b) to the bus speed.

40 mph, while decreased to about 0.29 time with changing the speed from 20 mph to 60 mph. Similarly, their relationship is not linear and the sensitivity of age of air to the bus speed was almost the same for different window opening scenarios as well. The only driver's window open scenario is the only case in which the air containing exhaust can infiltrate into the cabin through the back gaps and lead to self-pollution inside the bus cabin. Therefore, for the school buses, only opening the driver's window does not seem to be a good idea, because it could make the self-generated exhaust penetrate into the cabin more easily. Instead, it seems opening the middle windows might be an efficient way to avoid the back gap infiltration and mitigate the self-pollution.

### 3.3. Experimental results

To validate the model findings, Fig. 11 provides the ratio of in-cabin and on-road measurements (I/O) for UFPs and black carbon (BC) concentrations. The concentrations of UFPs and BC outside are almost always higher than those inside ( $I/O < 1$ ). This may be because the outside sampling tube is located closed to the near-

wake region of the bus and the outside concentration is effected by the bus own exhaust to some extent. I/O ratios of UFPs and BC agree well with the age of air distributions. As shown in Figs. 6 and 9, the age of air was found low in the middle section of a school bus in comparison to the front and the rear sections. Fig. 11 also provides the I/O ratio measured on local roadways at speed of  $30 \pm 29$  km/h and freeways at speed of  $87 \pm 37$  km/h; and effect of the speed on I/O ratio is not observable. This is because speeds of the school buses are not stable and the school buses make lots of stop-and-go trips to pick up children.

With respect to the I/O ratio measurements with all windows closed (Fig. 11a and d), opening driver's window increased the I/O ratio of both UFPs and BC concentrations (Fig. 11b and e). The increase of I/O ratio occurred throughout the school bus cabin, particularly in the rear section. This was because the infiltration through the back surface (i.e.,  $Q_{back-in}$ ) was particularly high for Case D, as shown in Table 1. Similar observations were repeated during data collection on local roadway (Fig. 11(b)) and freeway (Fig. 11(e)). As shown in Fig. 11c and f, when the middle windows were open, the I/O ratios of UFPs and BC further decreased

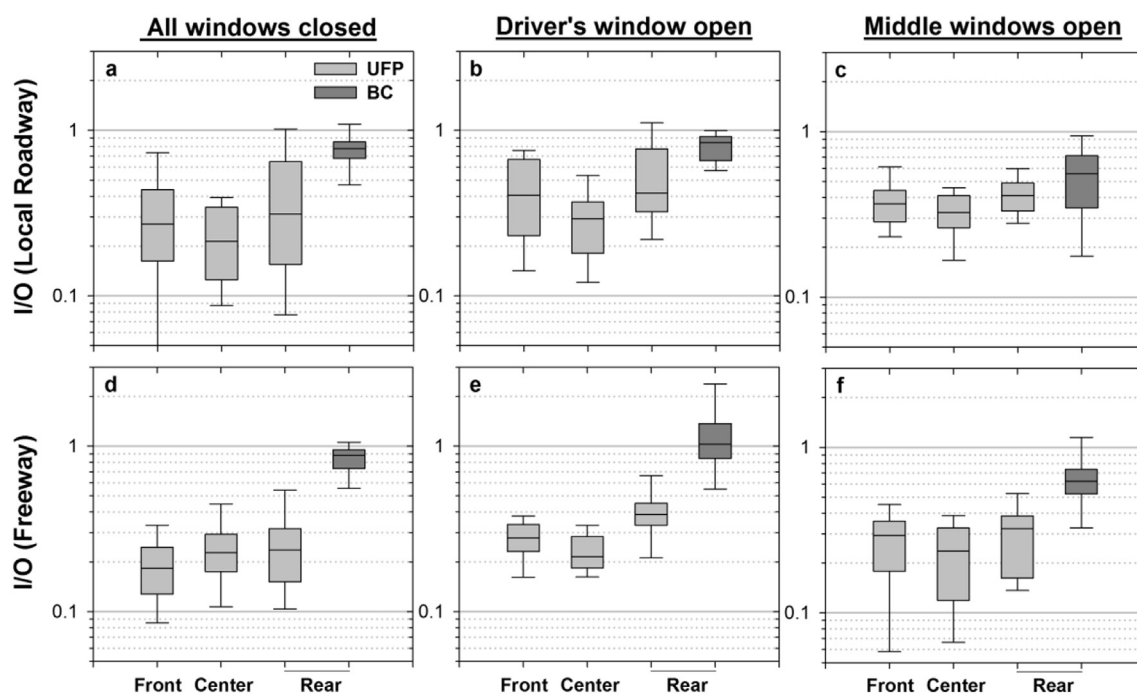


Fig. 11. UFPs and BC I/O ratio measurement data collected inside two school buses on local roadways (panels a–c) and freeways (panels d–f) with all windows closed (left), driver's window open (center), and middle windows open (right).



particularly in the rear section of school bus, because opening the middle windows could limit the infiltration through the rear surface of school bus. However, there was no significant decrease observed in the front and the middle section of school buses. This is likely because on-road traffic emissions from the motor-vehicles in front of the test school bus during data collection penetrated into the cabin through the middle windows.

This modeling study focuses on elucidating the effects of self-pollution under different window-opening scenarios, and it has some limitations. First, it should be noted, in heavy traffic, opening the bus windows may make the exhaust from other automobiles enter the bus and results in worse air quality. Therefore, the role of on-road traffic emissions on children's exposure, in comparison to self-pollution deserves further study. Secondly, this study didn't consider the mechanical ventilation in the school bus cabin. For the mechanical ventilation system, its form is various, and it will also affect the micro-environment and make effects of window openings hard to be separated. Thus, it is not taken into account in this study. Third, pollution from engine crankcase emissions can also lead to self-pollution pollution in older buses. Because in-use school buses have fewer gaps or leaks in their crankcases than the older ones (Zhang and Zhu, 2011), this aspect is not considered in this study either. In addition, unlike the typical school bus used in this study, most of modern coaches have air-tight cabins, and passages can only open the driver's window and side rear tiny window. Results from this study suggest this is not a very rational design because most of the exhaust pipes are located at the rear end, and the airflow could suck the exhaust into the cabin when the driver's window is open.

#### 4. Conclusions

This study adapted a CFD-based numerical model and field measurements to investigate the effect of window openings and bus speed on the airflow pattern and air quality inside school buses. By opening the side-windows in different positions, the airflow pattern and self-pollution level in the cabin was analyzed. The conclusions are as follows:

1. The proposed CFD-based method assigned the actual relative pressures to a certain percentage of boundary cells according to the effective area ratio of the gap boundaries. It was a trade-off between the computer capacity and basic need for describing geometry. This method can predict the airflow rate from the window gap infiltration and the results agree well with experimental data.
2. For the effect of the window openings, the self-exhaust can penetrate into the cabin through back door gaps more easily when only the driver's window was open. However, opening the middle windows could mitigate this phenomenon. Therefore, it is advised that the divers of school buses should not open the driver's window alone and at least make sure the side-windows in the middle are open. In addition, for all the scenarios, the age of air in the middle section of the cabin is lower because most of the air enters through the middle gaps and windows. Lower UFPs I/O ratio was also observed in the middle section of the school bus in the experiment.
3. For the effect of the bus speed, higher speed (from 20 mph to 60 mph) resulted in a higher ventilation rate of the cabin (up to 3.4 times) and a lower average value of age of air for the whole cabin (down to 0.29 time) corresponding to more observable "pump" effect. However, more air would penetrate into the cabins through the back window gaps at a higher speed.

The current work focused on the school bus because children are a susceptible subpopulation, but the theoretical framework in this study can be generalized to other types of buses, and the results can be potentially useful to policy makers and manufacturers.

#### Acknowledgement

This work is supported by the Natural Science Foundation of Jiangsu Province (Grants No. BK20171015). The experimental work described in this article was funded by grant number A-00909414-0 from the U.S. Environmental Protection Agency's Clean Air Technology Initiative awarded to the South Coast Air Quality Management District. Any opinions, findings, conclusions, or recommendations expressed in this report are those of the authors and do not necessarily reflect the views of the U.S. Environmental Protection Agency or the South Coast Air Quality Management District. Fei Li also would like to thank the National Natural Science Foundation of China (No. 51708286 and No. 51508267).

#### Appendix A. Supplementary data

Supplementary data related to this article can be found at <http://dx.doi.org/10.1016/j.atmosenv.2017.08.053>.

#### References

- Abanto, J., Barrero, D., Reggio, M., Ozell, B.T., 2004. Airflow modelling in a computer room. *Build. Environ.* 39, 1393–1402.
- Ansys, A.F., 2011. 14.0 Theory Guide. ANSYS inc.
- Behrentz, E., Fitz, D.R., Pankratz, D.V., Sabin, L.D., Colome, S.D., Fruin, S.A., Winer, A.M., 2004. Measuring self-pollution in school buses using a tracer gas technique. *Atmos. Environ.* 38, 3735–3746.
- Fitz, D.R., Winer, A.M., Colome, S., 2003. Characterizing the Range of Children's Pollutant Exposure during School Bus Commutes. School of Public Health University of California, Los Angeles.
- Hu, X.J., Ren, F.T., Yang, B., Guo, P., 2012. Effect of sunroofs and side windows on aerodynamic characteristics of transit bus. *Appl. Mech. Mater.* 224, 333–337.
- Kale, S., Veeravalli, S., Puneekar, H., Yelmule, M., 2007. Air flow through a non-airconditioned bus with open windows. *Sadhana* 32, 347–363.
- Kim, J., 2004. Ambient air pollution: health hazards to children. *Pediatrics* 114, 1699–1707.
- Lee, E.S., Fung, C.-C.D., Zhu, Y., 2015. Evaluation of a High Efficiency Cabin Air (HECA) filtration system for reducing particulate pollutants inside school buses. *Environ. Sci. Technol.* 49, 3358–3365.
- Li, F., Lee, E.S., Liu, J., Zhu, Y., 2015. Predicting self-pollution inside school buses using a CFD and multi-zone coupled model. *Atmos. Environ.* 107, 16–23.
- Li, F., Liu, J., Ren, J., Cao, X., Zhu, Y., 2016. Numerical investigation of airborne contaminant transport under different vortex structures in the aircraft cabin. *Int. J. Heat Mass Tran.* 96, 287–295.
- Lin, B., Wang, X.T., Hu, X., 2012. Research on the effect of natural ventilation on buses in summer based on CFD numerical simulation method. *Adv. Mater. Res.* 361, 1056–1060.
- Maybee, K., MacKinnon, B., Kerr, B., 2010. Evaluation of the Levels of Diesel-related Pollutants from School Buses while Transporting Children. New Brunswick Lung Association.
- Mott, L., Fore, D., Curtis, J., Solomon, G., Hanson, B., 1997. Our Children at Risk: the 5 Worst Environmental Threats to Their Health, NRDC Toxic Chemicals & Health. NRDC.
- Rim, D., Siegel, J., Spinhirne, J., Webb, A., McDonald-Buller, E., 2008. Characteristics of cabin air quality in school buses in Central Texas. *Atmos. Environ.* 42, 6453–6464.
- Roache, P.J., 1994. Perspective: a method for uniform reporting of grid refinement studies. *Transactions-American Soc. Mech. Eng. J. Fluids Eng.* 116, 405–405.
- Sabin, L.D., Behrentz, E., Winer, A.M., Jeong, S., Fitz, D.R., Pankratz, D.V., Colome, S.D., Fruin, S.A., 2004. Characterizing the range of children's air pollutant exposure during school bus commutes. *J. Expo. Sci. Environ. Epidemiol.* 15, 377–387.
- U.S.EPA, 2012. <https://www.epa.gov/cleandiesel/clean-school-bus>.
- Vu, T.V., Delgado-Saborit, J.M., Harrison, R.M., 2015. Review: particle number size distributions from seven major sources and implications for source apportionment studies. *Atmos. Environ.* 122, 114–132.
- Zhang, Q., Fischer, H.J., Weiss, R.E., Zhu, Y., 2013. Ultrafine particle concentrations in and around idling school buses. *Atmos. Environ.* 69, 65–75.
- Zhang, Q., Zhu, Y., 2010. Measurements of ultrafine particles and other vehicular pollutants inside school buses in South Texas. *Atmos. Environ.* 44, 253–261.
- Zhang, Q., Zhu, Y., 2011. Performance of school bus retrofit systems: ultrafine

- particles and other vehicular pollutants. *Environ. Sci. Technol.* 45, 6475–6482.
- Zhang, T.T., Lee, K., Chen, Q.Y., 2009. A simplified approach to describe complex diffusers in displacement ventilation for CFD simulations. *Indoor Air* 19, 255–267.
- Zhu, S., Demokritou, P., Spengler, J., 2010. Experimental and numerical investigation of micro-environmental conditions in public transportation buses. *Build. Environ.* 45, 2077–2088.
- Zhu, S., Srebric, J., Spengler, J.D., Demokritou, P., 2012. An advanced numerical model for the assessment of airborne transmission of influenza in bus micro-environments. *Build. Environ.* 47, 67–75.